Title

THREE-DIMENSIONAL RECONSTRUCTION IN PLANAR POSITRON CAMERAS USING FOURIER DECONVOLUTION OF GENERALIZED TOMOGRAMS

Author

Tam, K.C.

Publication Date

1977-10-01

Presented at the IEEE Nuclear Science Symposium, San Francisco, CA, October 19 - 21, 1977; also Submitted to IEEE Transactions on Nuclear Science

LBL-6774

THREE-DIMENSIONAL RECONSTRUCTION IN PLANAR POSITRON CAMERAS USING FOURIER DECONVOLUTION OF GENERALIZED TOMOGRAMS

K. C. Tam, G. Chu, V. Perez-Mendez, and C. B. Lim

October 1977

Prepared for the U. S. Department of Energy
under Contract W-7405-ENG-48

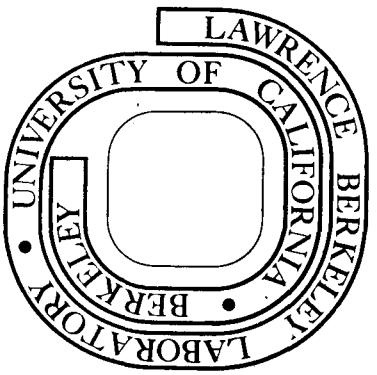

DISCLAIMER

THREE-DIMENSIONAL RECONSTRUCTION IN PLANAR POSITRON CAMERAS USING FOURIER DECONVOLUTION OF GENERALIZED TOMOGRAMS

K.C. Tam, G. Chu, V. Perez-Mendez and C.B. Lim
Lawrence Berkeley Laboratory
and
University of California, San Francisco

Abstract

A computational method for obtaining Three-Dimensional reconstructions of positron emitting radionuclei distributions using a Planar Positron camera is described. The method involves the use of a Filtered Fourier Deconvolution Method. Construction of Generalized Tomograms capable of emphasizing the large angle events is introduced. The finite size of the Positron Camera detector and its effect on the reconstruction are discussed.

I. Introduction

In nuclear medicine, positron cameras are used for imaging medical disorders such as brain tumors by locating the two coincident back-to-back gamma rays emitted from the radioisotope injected into the patient's body. These two gamma photons, which are generated when the positrons produced in the β decay processes are annihilated at rest by the electrons in the immediate vicinity, are detected by the positron camera in coincidence, and their positions of interaction with the detectors recorded (Figure 1). Each pair of annihilation gammas defines a straight line in space, with the position of the radioactive nuclide which has just undergone the decay lying somewhere along the line. In order to deduce the radioisotope distribution from these data, one simple approach is to construct the tomograms which are the distribution of the intersection points of the annihilation gammas with different planes. This method, however, suffers from severe blurring due to superimposition of off-plane activities. In this paper we shall describe a reconstruction technique for recovering 3-dimensional image from the data.

II. Fourier Deconvolution

If the number of straight lines defined by the annihilation gamma pairs becomes large they will form a pattern, or scalar field, which we shall denote as $\phi(\underline{r})$, in space. This scalar field $\phi(\underline{r})$ is a superimposition of the scalar fields $\phi_o(\underline{r})$ generated by each point emitter in the radioisotope distribution (Figure 2). If $\phi_o(\underline{r})$ is space invariant, i.e. it is a function only of the position relative to the point emitter and independent of the position of the point emitter itself, the following equation holds

$$\phi(\underline{r}) = \int \rho(\underline{r}')\phi_o(\underline{r}-\underline{r}')d^3\underline{r}'$$

where $\rho(\underline{r})$ is the radioisotope density distribution. Using the convolution theorem we get

$$\Phi(\underline{p}) = R(\underline{p})\Phi_o(\underline{p})$$

where

$$\Phi(\underline{p}) = \int \phi(\underline{r})e^{2\pi i\underline{p}\cdot\underline{r}}d^3\underline{r}$$

$$\Phi_o(\underline{p}) = \int \phi_o(\underline{r})e^{2\pi i\underline{p}\cdot\underline{r}}d^3\underline{r}$$

$$R(\underline{p}) = \int \rho(\underline{r})e^{2\pi i\underline{p}\cdot\underline{r}}d^3\underline{r}$$

and $\underline{p}$ denotes the momentum or spatial frequency space. Thus the density $\rho(\underline{r})$ can be found by the inverse transform

$$\rho(\underline{r}) = \int R(\underline{p})e^{2\pi i\underline{p}\cdot\underline{r}}d^3\underline{p} \qquad (1)$$

with

$$R(\underline{p}) = \frac{\Phi(\underline{p})}{\Phi_o(\underline{p})} \qquad (2)$$

III. Possible Point Response Functions

The space invariant point response function $\phi_o(\underline{r})$ can be constructed in a number of ways from a knowledge of the location of the annihilation gamma pairs emitted from a point source and the angle θ it makes with the z-axis. Figure 3 shows one way to construct such a point response function. A volume element is used to measure the total length of the line segments that are contained within its volume. The average total length of these line segments defines the point response function at that position. Another $\phi_o(\underline{r})$ which is easier for both computation and construction is shown in Figure 4. Instead of a volume element, a small area element with its normal along the z-axis is used as the measuring scale. The number of lines passing through the area element is taken as a definition of the point response function. These are just the conventional tomograms obtained by back projecting the data.

We can generalize the last definition of $\phi_o(\underline{r})$ to an entire family of point response functions by making use of the angle information inherent in the positron camera data. Each line passing through the area element is weighted by a factor depending on the angle θ the line makes with the z-axis, e.g. $\cos^n\theta$, $\sin^n\theta$, etc. This results in generalized tomograms in which large angle and small angle events are given different emphasis, and thus gives rise to the possibility of improving the quality of the reconstruction by weighting the large angle events more.

To complete the discussion of the point response function, we notice that the detection apparatus does not usually subtend the full 4π steradian solid angle. As a consequence each point in the density distribution has a local cone of detection; which means any gamma pair emitted from that point cannot be recorded by the positron camera if it falls outside the local cone. The size of the local cone of detection varies with the position of the point emitter. This makes the point response function space variant.

One way to remove this dependence is to use only those gamma pairs which make an angle with the z-axis smaller than a certain limit set by the minimum local cone of detection in the density distribution. This principle is illustrated in Figure 5. The local cone of detection at $\underline{r}_1$ is smaller than that at $\underline{r}_2$; but if we use only those events falling within the shaded cones which have the same size as the smaller of the two local cones at $\underline{r}_1$ and $\underline{r}_2$, the point response functions generated at these two positions would again be the same.

IV. Removal of Noise Instabilities

The reconstruction method described by equations (1) and (2) only works if there is no noise. If the data contains noise, the solution of the equations is unstable, and, as shown by Phillips (1), large oscillations would appear in the solution when the cell size used in the computation is made small enough.

A way to deal with the noise instabilities has been described in a previous paper (2) in which the treatment of noise by Phillips (1) was recast. By imposing the smoothness condition

$$\int (\nabla^2 \rho(\underline{r}))^2 d^3\underline{r} = \text{minimum} \qquad (3)$$

on the solution $\rho(\underline{r})$, equation (2) is modified to

$$R(\underline{p}) = \frac{\Phi(\underline{p})}{\Phi_o(\underline{p}) + \frac{\gamma(2\pi)^4 p^4}{\Phi_o(\underline{p})}} \qquad (4)$$

in the presence of noise. Here $\gamma(>0)$ is an adjustable parameter which depends on the noise level. In the case of no noise, $\gamma = 0$, and equation (4) reduces back to equation (2).

The modification made in equation (4) can be viewed as the action of a low spatial frequency pass filter. In general, the signal component in $\phi(\underline{p})$ decreases in magnitude with frequency, whereas the power spectrum of the noise component is essentially flat. Thus the noise component dominates in the high frequency range. This high frequency noise is further amplified in dividing by $\Phi_o(\underline{p})$, which is usually also a small quantity at high frequency (3).

The additional term in equation (4)

$$\frac{\gamma(2\pi)^4 p^4}{\Phi_o(\underline{p})}$$

is negligible at low frequency compared to $\Phi_o(\underline{p})$, but increases rapidly in magnitude with frequency as both p^4 increases and $|\Phi_o(\underline{p})|$ decreases. Thus the information at low frequency is undistorted whereas the noise at high frequency is suppressed.

The above treatment can be generalized to give a family of frequency filters of the form

$$\Phi_o(\underline{p}) + \frac{\gamma(2\pi)^m p^m}{\Phi_o(\underline{p})} \qquad (5)$$

where m is a positive integer which controls the sharpness of the filter. m corresponds to different powers of $\nabla^2\rho(\underline{r})$ in the smoothness condition (3). By adjusting m an optimum filter can be constructed to suit the noise characteristics of each imaging system.

V. Implementation

As the actual computation is done by digital computers, the digital version of the algorithm should be used. The region of space in the vicinity of the density distribution is divided into a 3-dimensional lattice, $N_x \cdot N_y \cdot N_z$, with spacings between the lattice sites δ_x, δ_y, δ_z. Such digitization introduces errors into the results of the Fourier transforms: the finite lattice spacing gives rise to 'aliasing', and the truncation causes 'leakage' (4). The former is minimized by making the lattice spacing δ_x, δ_y, δ_z small enough, while the latter can be reduced by premultiplying the scalar fields $\phi(\underline{r})$ and $\phi_o(\underline{r})$ by window functions (5) before taking the transforms. In our work gaussian window functions appear to give the best results, but the type of window does not seem to be critical. Windowing is not required when taking the inverse transform of $R(\underline{p})$, as $R(\underline{p})$ is a periodic function with period equal to the truncation interval in which case there is no leakage.

The system transfer function $\Phi_o(\underline{p})$ for an imaging system needs to be computed only once. Most of the computer time in the reconstruction is spent in the construction of the scalar field $\phi(\underline{r})$ and taking two Fourier transforms. For a CDC 7600 computer with a cycle time of 27.5 ns, Fast Fourier transform of an 32 X 32 X 32 X array take only 0.2 sec,* and only 10.6 sec for an 64 X 64 X 60 array.** If the computing has to be done on a small machine with limited high speed storage, data could be stored in slower memory devices such as tape or drum. Separate transforms are computed and then combined (6,7,8).

VI. Results

The algorithm has been applied to a computer generated phantom and also on real data taken from the multi-wire proportional chamber (MWPC) planar positron camera at the University of California, San Francisco. The results are shown in Figures 6-12. In each figure we have shown a series of planes parallel to the detectors, starting from the central plane and working outward in one direction. The distance between the planes is equal to the lattice spacing S_z.

The simulated phantom (Figures 6-8) consists of a 'skull region' corresponding to the blood supply for the brain, a 'brain' and a hypothetical 'tumor'. The 'skull region' was a spherical shell 3 cm thick, with an inner radius of 18 cm and an outer radius of 21 cm, and with an activity concentration of 5:1. The 'tumor' was a sphere located off-centre in the 'brain', with a radius of 3.6 cm and a concentration of 10:1. The detection system is made up of two square detectors of area 85 X 85 cm^2 separated by 50 cm. In the reconstruction we have chosen a lattice of dimensions 32 X 32 X 32, and the lattice distances were 2.5 X 2.5 X 5.0 cm^3.

Figure 6 shows the actual density distribution. Figure 7 shows the results obtained by a simple back projection of the data. Only those events lying inside the minimum cone of detection are used, to remove any bias as one moves out toward the edges. The tumor can still be seen, but the image is blurred by the off-plane activities. Furthermore, the tumor has cast a recognizable shadow on at least two other planes, where it does not exist.

Figure 8 shows the results obtained using our reconstruction algorithm. Here we have used the generalized tomograms weighted by $\cos^{-3}\theta$ as the scalar fields. The point response function was calculated analytically. $m = 4$ was used in the frequency filter and the otpimum value of γ was found to be 8.02×10^{-4}. The image of the tumor appears quite clearly, and shadowing onto other planes has disappeared.

Figures 9-12 show the results for the real data taken for a cylinder head-phantom with two simulated tumors. One tumor has activity concentration of 5:1, and the other 10:1. The head-phantom was immersed in a container filled with Ga-68 (concentration 5:1) simulating the peripheral activity around the 'skull'. The "skull" is in the form of a cylindrical shell which

*Using the Fast Fourier Transform Algorithm by K.F. Subhani and Frank Chu, private communication.

**Using the Fast Fourier Transform Algorithm by Singleton (9), and a supplementary program for transforming real data by the same author and modified by K.C. Tam, private communication.

is 1.5 cm thick and 16.5 cm high, with an inner radius of 7.5 cm. The two tumors are also cylindrical in shape, with 1 cm radius and 4 cm height.

For this phantom we have used a lattice of dimensions 64 X 64 X 60, and the lattice spacings were 5 X .5 X 1.0 cm^3. The detection system was made up of four large area MWPCs equipped with Pb-converters, two on each side of the phantom. Each chamber has an area of 48 X 48 cm^2. The distance between the inner MWPC pair is 55.6 cm, and 63.6 cm for the outer pair.

Figure 9 shows the results obtained by simple back projection with solid angle limitation. The images of the tumors are almost completely buried under the off-plane activities plane and can hardly be seen. Figure 10 is obtained from Figure 9 by subtracting from the content of each cell 55% of the peak activity. This helps to bring out the contrast, and the tumors faintly appear near the central planes.

Figure 11 shows the results obtained by our reconstruction algorithms using generalized tomograms weighted by $\cos^{-4}\theta$ as the scalar fields. The point response function that we used was obtained by fitting a smooth analytic function to the experimentally measured values. The parameters used in the frequency is m = 10, and the corresponding optimum γ is 71.7. The two tumors and the skull region are clearly visible, and well separated. The left-right asymetry in Figures 9-10 is also removed.

As a comparison, the reconstruction using conventional tomograms as scalar fields are shown in Figure 12. The parameters used in the frequency filter are also m = 10 and γ = 71.7. The two tumors and the skull also appear distinctly, but the two tumors are not so well separated as in Figure 11. This agrees with the remark in Section III that putting more weight on the large angle events should improve the reconstruction.

VII. Conclusion

The Fourier deconvolution scheme described above provides a simple method for reconstructing the images from the positron camera data. The use of an optimum weighting factor $\cos^n\theta$ in constructing the generalized tomograms used as scalar fields results in better resolution through emphasizing the large angle events. The possibility of adjusting the value of m in the frequency filter offers additional flexibility in the reconstruction. It also suggests the possible use of other frequency filters such as the minimum mean square error filter (10) and the homomorphic filter (11). Work has been started in this direction. Also started is the scheme to make use of all the data in the reconstruction by an one-step iteration in which the maximum cone of detection rather than the minimum one is used in constructing the scalar fields.

Acknowledgments

We would like to take this opportunity to thank Dr. F. Chu of Physical Dynamics Inc. for making available the program for Fast Fourier Transform. We also wish to thank Dr. B. Macdonald for many helpful discussions.

This work was supported by the U. S. Department of Energy under the auspices of the Division of Physical Research.

References

1. Phillips, D.L., J. Assoc. Comput. Mach., 9(1962)84.

2. Chu, G., and Tam, K.C., Phys. Med. Biol., 22(1977) 245.

3. Pizer, S.M., Brownell, G.L., and Chester, D.A., 1974, Instrumentation in Nuclear Medicine (New York and London: Academic Press) Vol. 2: p. 238.

4. Brigham, O., 1974, The Fast Fourier Transform (New York: Prentice Hall).

5. Blackman, R.B., and Tukey, J.W., 1958, The Measurement of Power Spectra from the Point of View of Communications Engineering (New York: Dover) p. 98.

6. Brenner, N.M., IEEE Trans. Audio and Electroacoustics, AU-17(1969)128.

7. Buijs, H.L., Applied Optics, 3(1969)211.

8. Singleton, R.C., IEEE Trans. Audio and Electroaucoustics, AU-15(1967)91.

9. Singleton, R.C., IEEE Trans. Audio and Electroacoustics, AU-17(1969)93.

10. Helstrom, C.W., J. Opt. Soc. Amer., 57(1967)297.

11. Oppenheim, A.V., Schafer, R.W., and Stockham, T.G., Proc. IEEE, 56(1968)1264.

Figure Captions

Fig. 1. Schematic figure of planar positron camera.

Fig. 2. Scalar field $\phi(\underline{r})$ formed by the annihilation gamma pairs.

Fig. 3. Point response function defined by a volume element.

Fig. 4. Point response function defined by an area element with its normal along the z-axis.

Fig. 5. Making the point response space invariant by solid angle limitation. Only those gamma pairs falling within the minimum local cone of detection (the shaded cones) are used.

Fig. 6. A computer generated phantom simulating a brain tumor. The skull is 3cm thick and has an inner radius of 18cm. The tumor has a radius of 3.6cm. The concentration is 5:1 for the skull and 10:1 for the tumor. Each picture element is $2.5\times2.5\text{cm}^2$. The planes are 5cm apart.

Fig. 7. Images of the computer generated phantom by simple back projection.

Fig. 8. Reconstruction of the computer generated phantom by Fourier deconvolution. The scalar fields used in the reconstructions are generalized tomograms weighted by $\cos^{-3}\theta$. The filtering parameters are: $m = 4, \gamma = 8.02\times10^{-4}$.

Fig. 9. Back projection images of a real phantom which consists of a cylindrical shell to simulate a skull, and 2 cylindrical tumors. The shell is 1.5cm thick, 16.5cm high, and has an inner radius of 7.5cm. Each tumor is 4cm high and has a radius of 1cm. The concentration ratio is 5:1 for the skull and one tumor, and 10:1 for the other. Each picture element is $0.5\times0.5\text{cm}^2$. The planes are 1cm apart.

Fig. 10. Back projection of the data from the real phantom with 55% background subtraction.

Fig. 11. Reconstruction of the real phantom by Fourier deconvolution. The scalar fields used are generalized tomograms weighted by $\cos^{-4}\theta$. The filtering parameters are: $m = 10$, $\gamma = 71.7$.

Fig. 12. Reconstruction of the real phantom by Fourier deconvolution. Tomograms are used as scalar fields in the reconstruction. The filtering parameters are: $m = 10$, $\gamma = 71.7$.

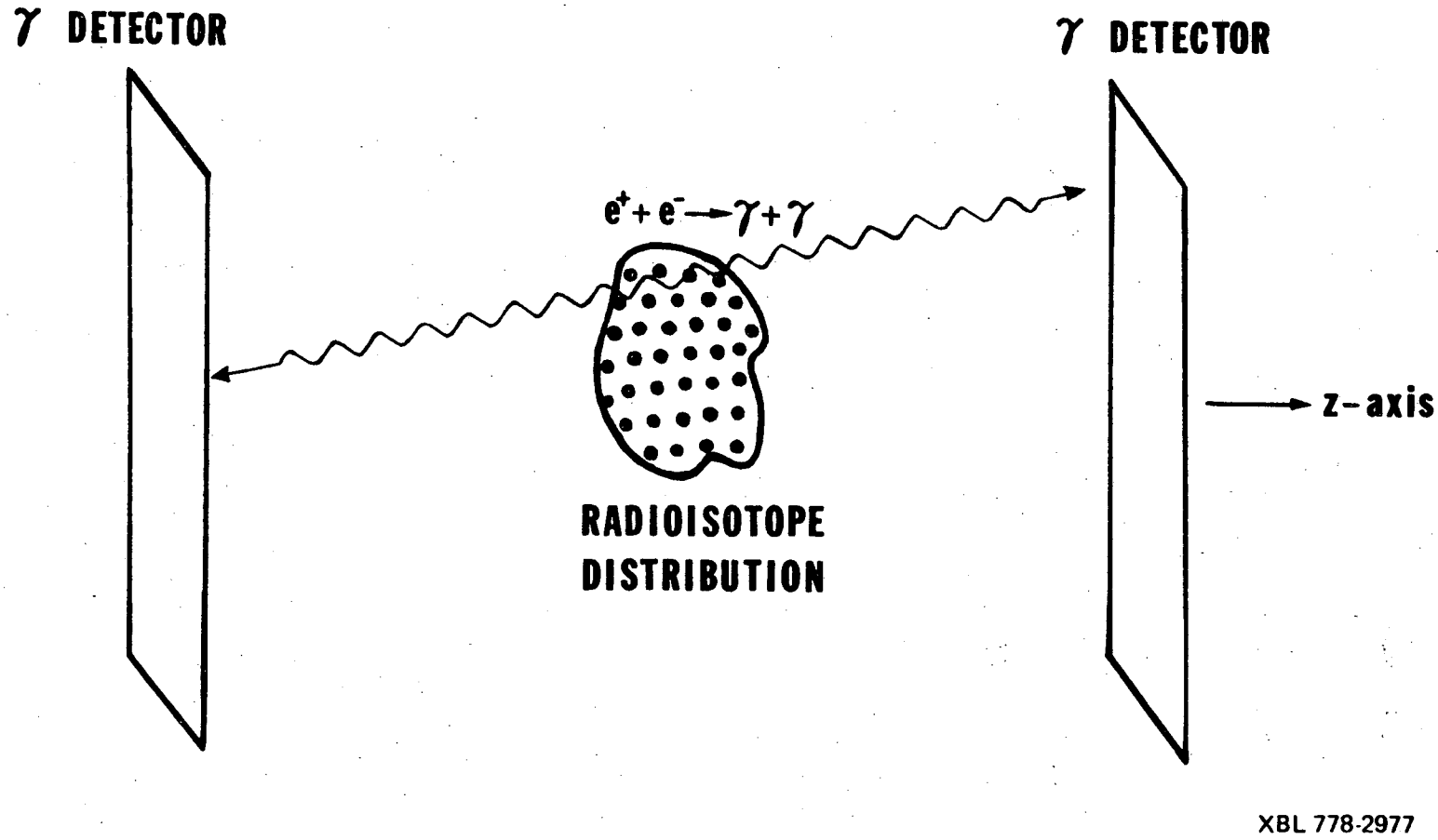
γ DETECTOR
γ DETECTOR
e⁺+e⁻→γ+γ
z-axis
RADIOISOTOPE
DISTRIBUTION
XBL 778-2977

Figure 1

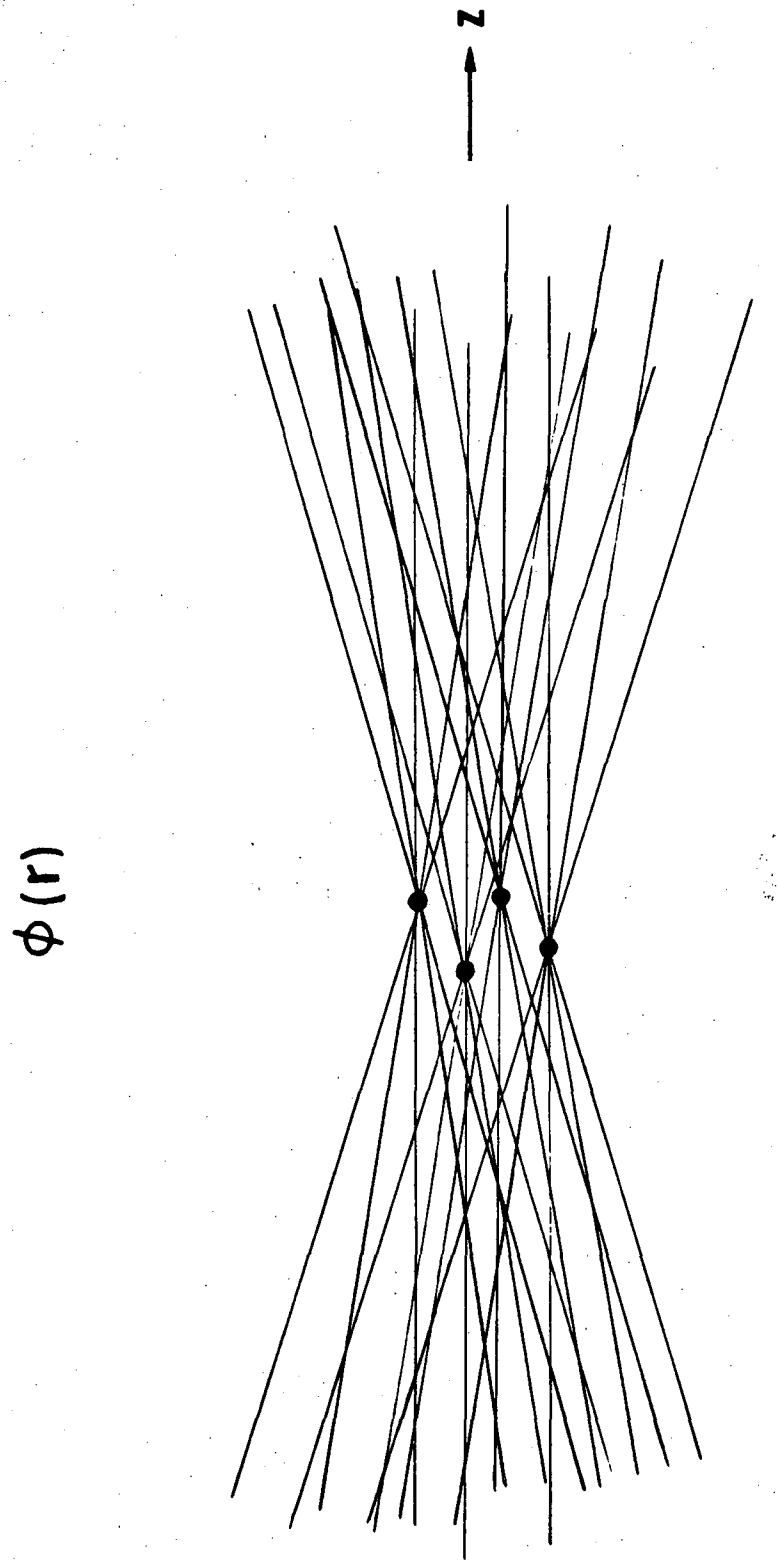

XBL 778-2979

Figure 2

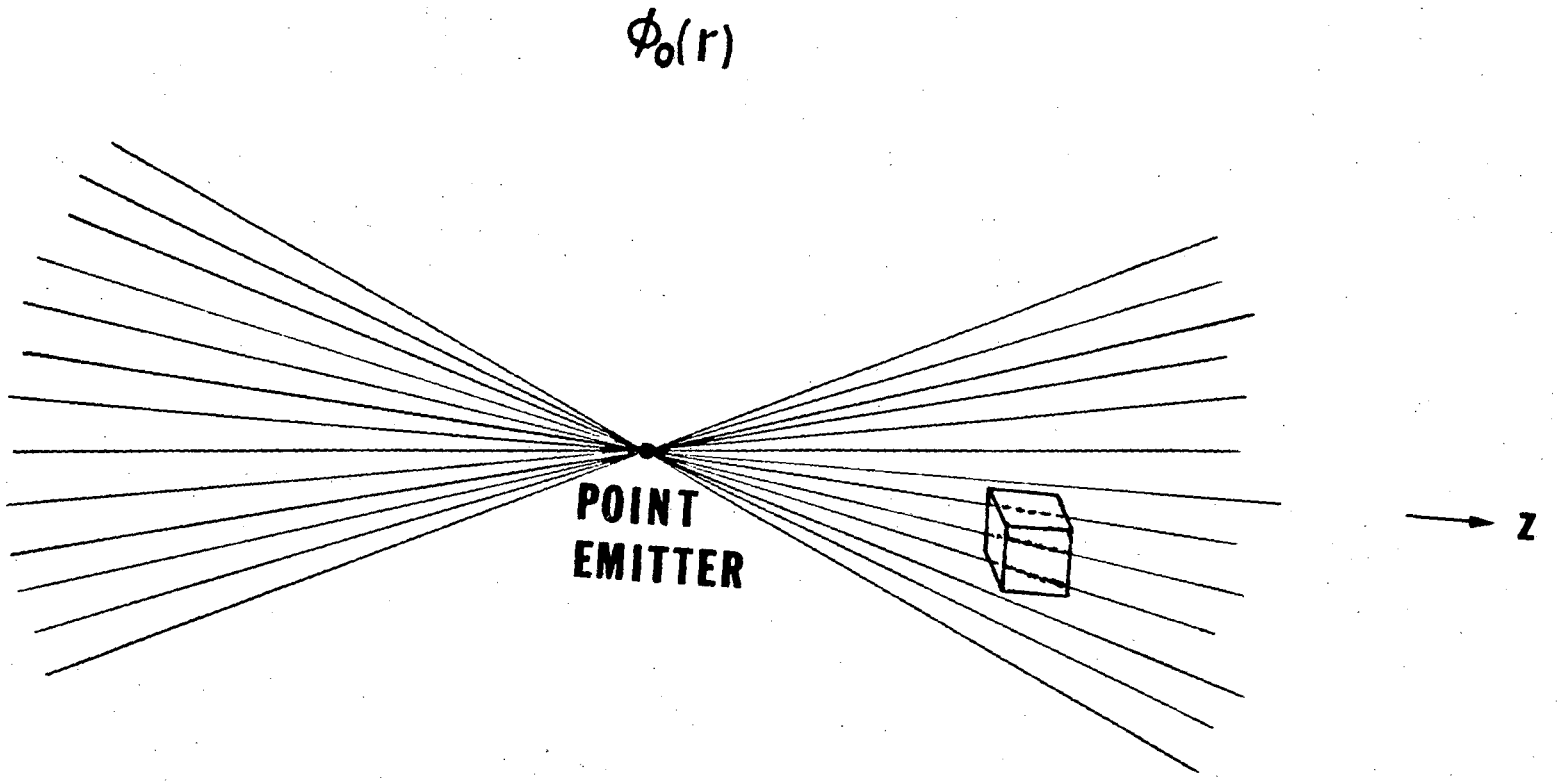

Figure 3

XBL 778-2980

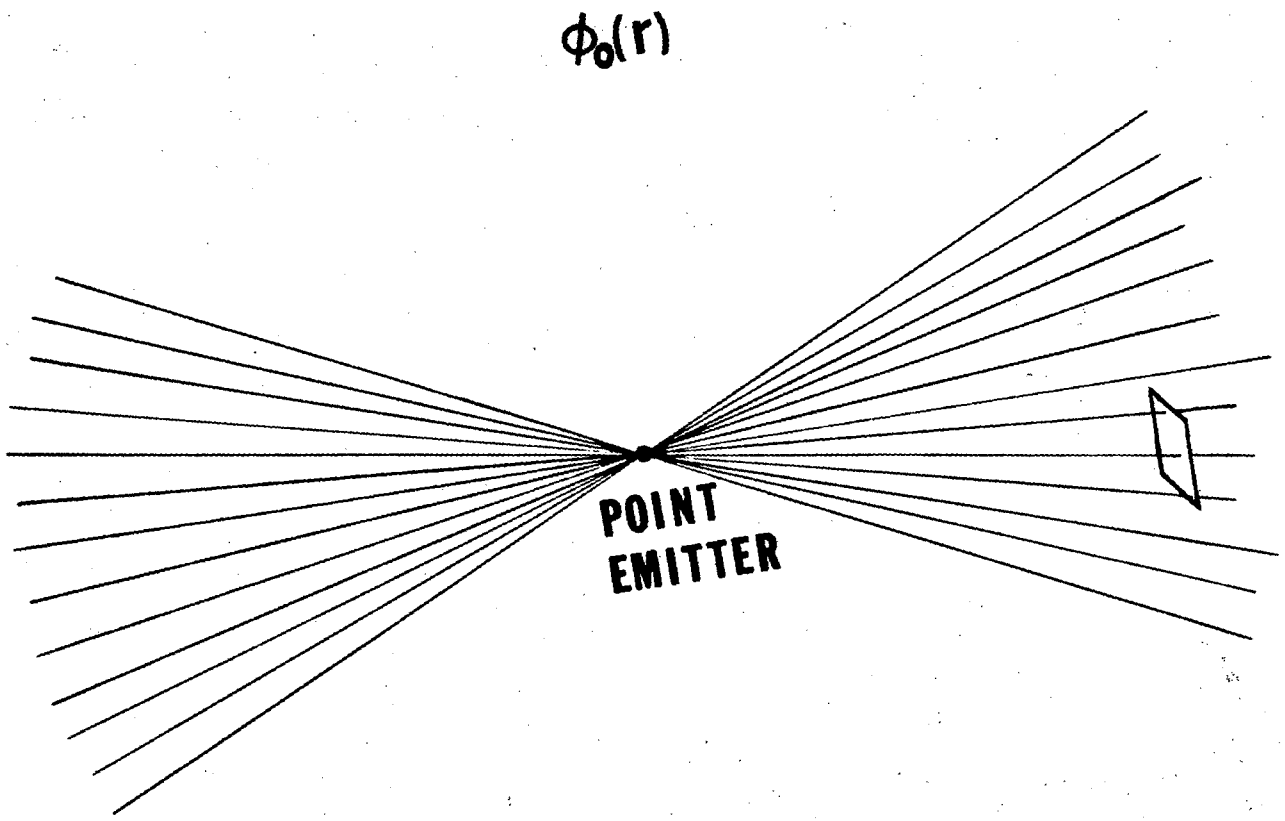

XBL 778-2978

Figure 4

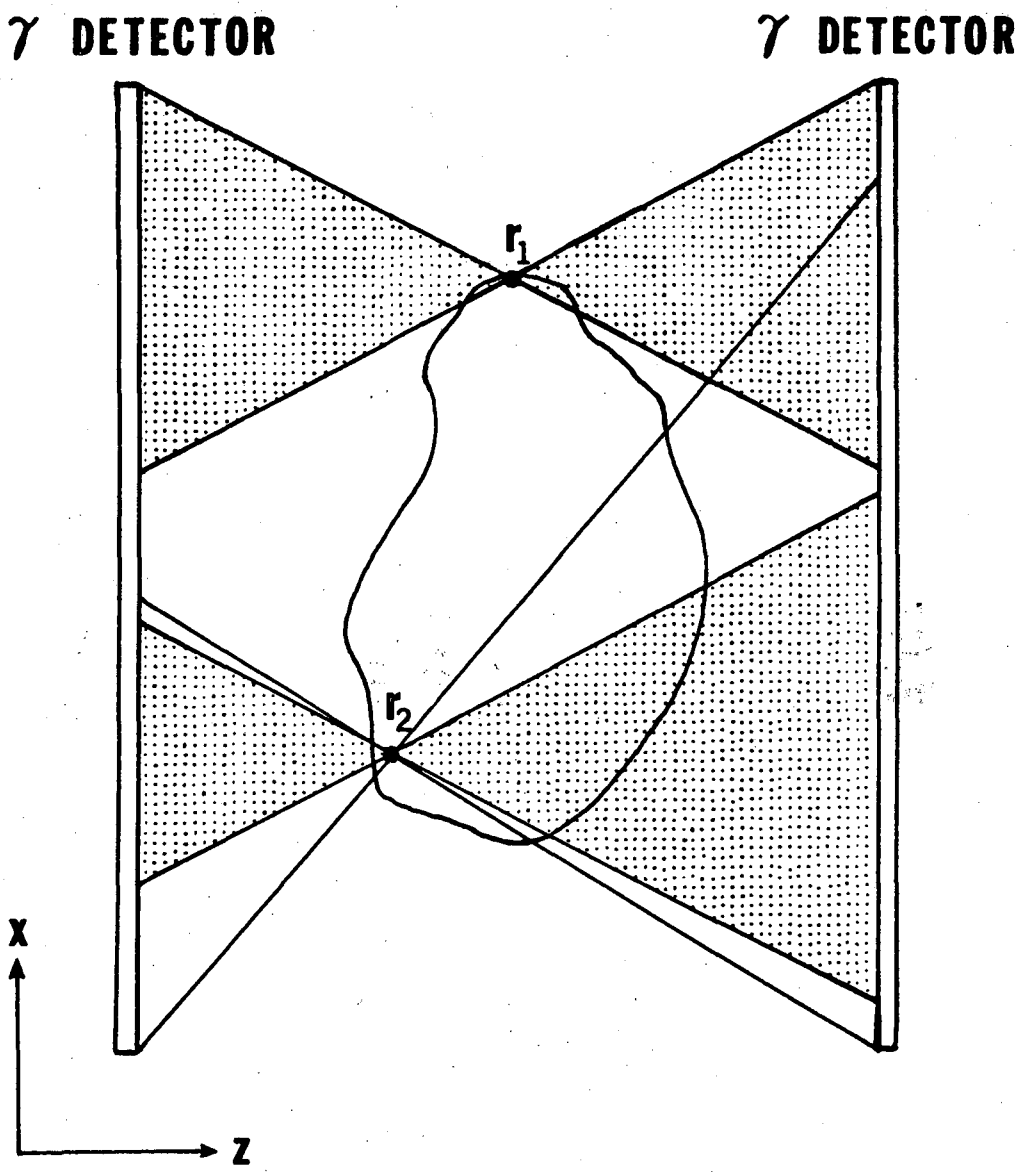

XBL 778-2976

Figure 5

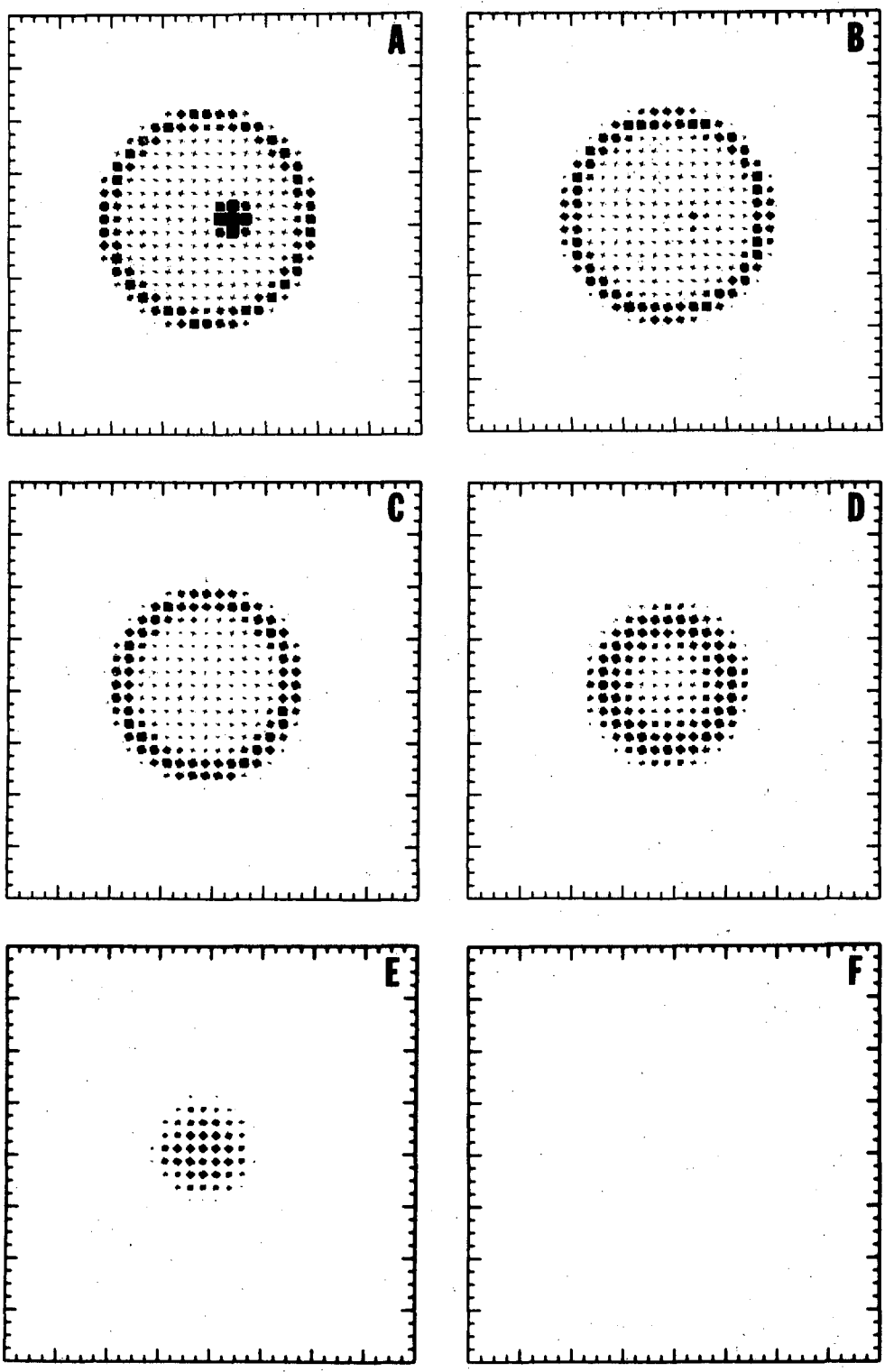

XBL 7710-10320

Fig. 6

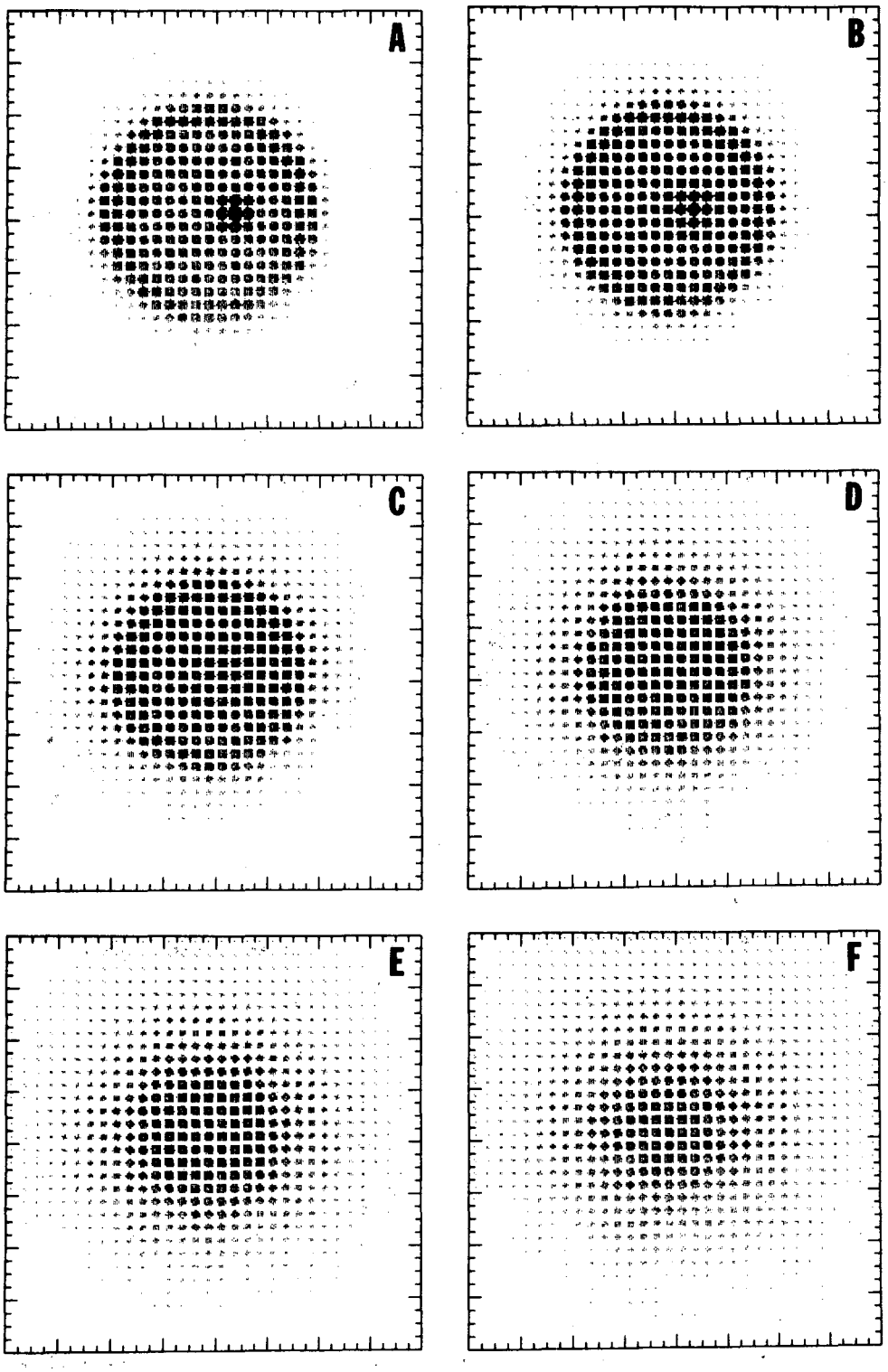

XBL 7710-10321

Fig. 7

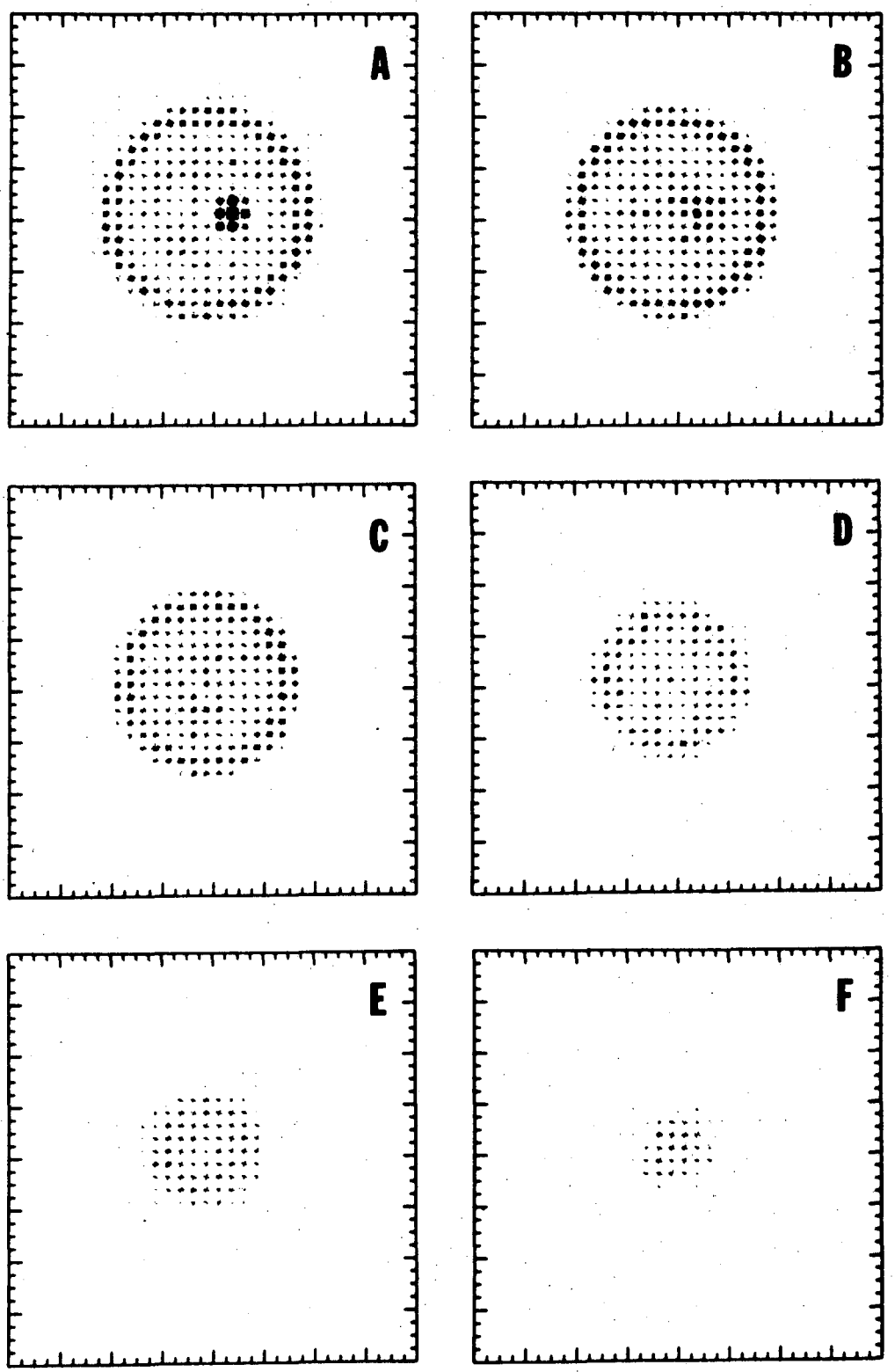

XBL 763-890

Figure 8

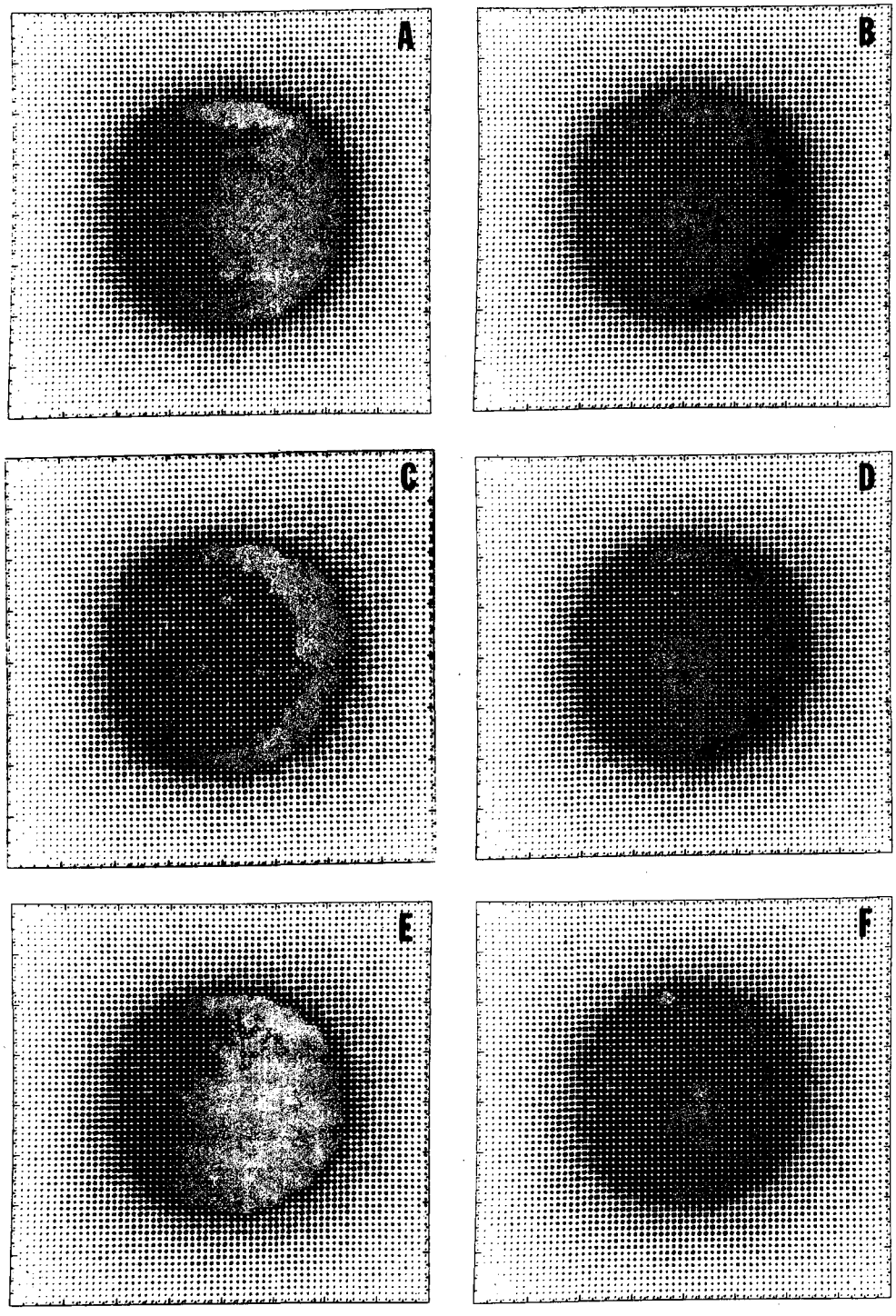

XBL 7710-10322

Fig. 9

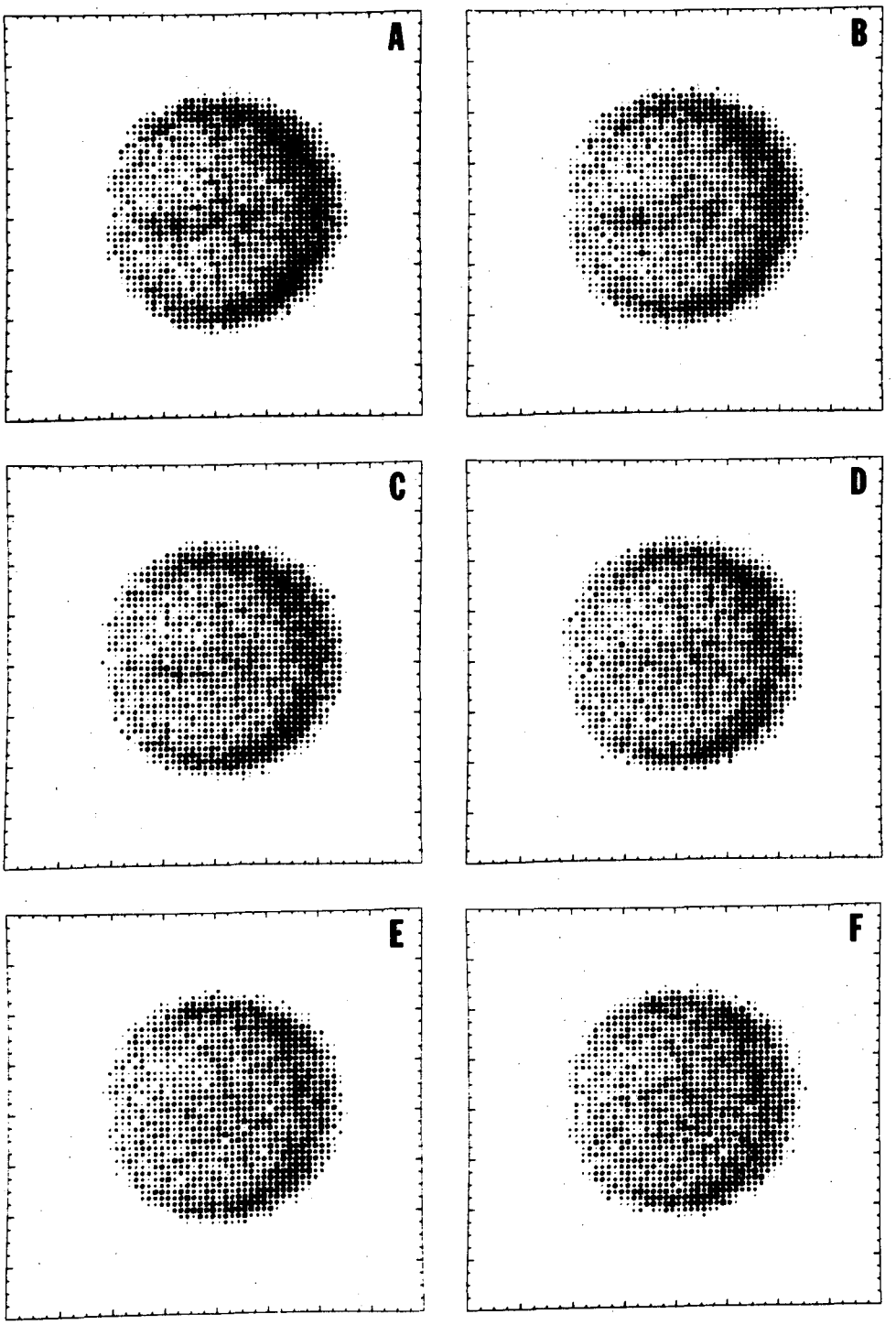

XBL 7710-10318

Fig. 10

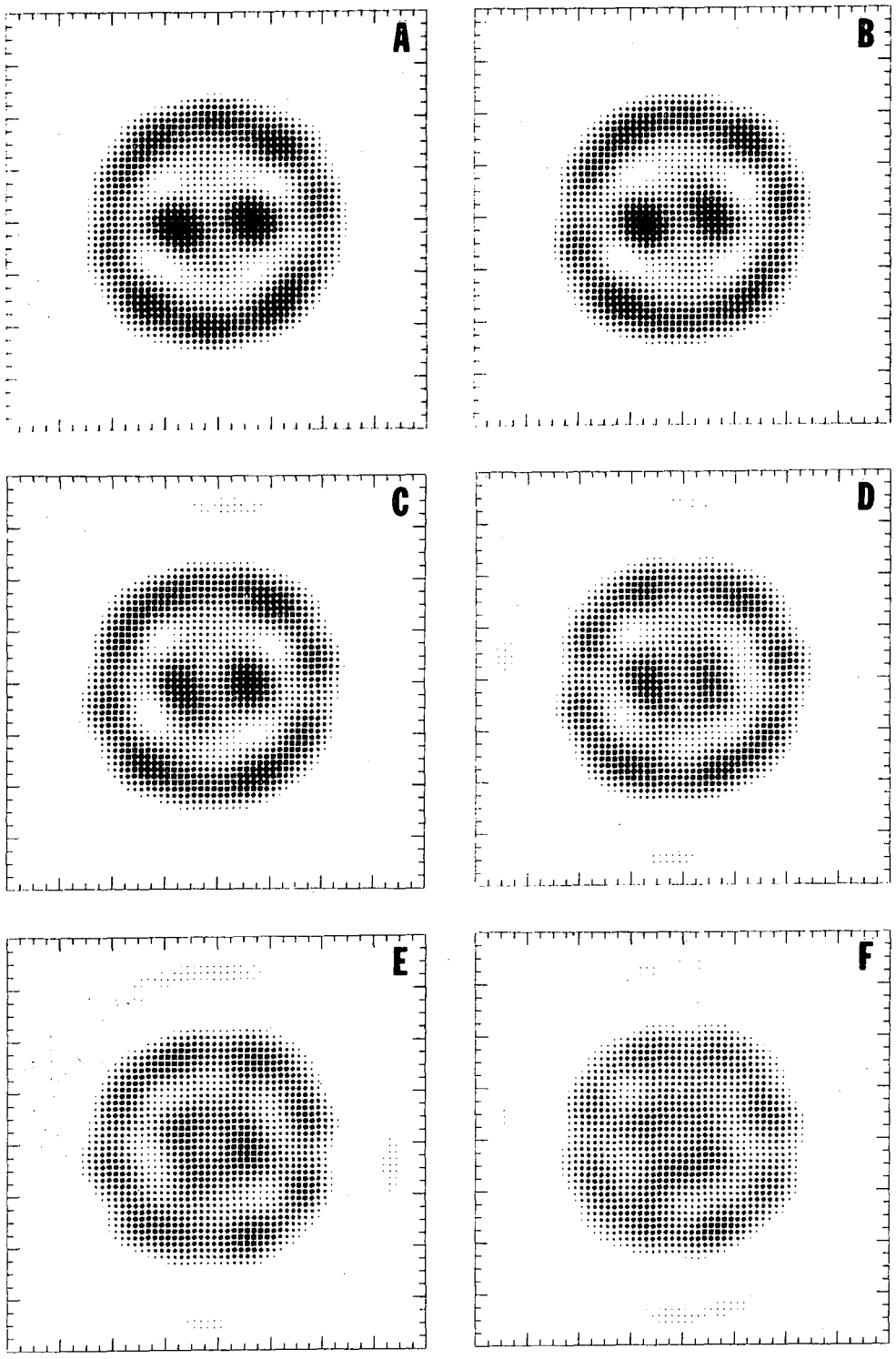

XBL 7710-10319

Fig. 11

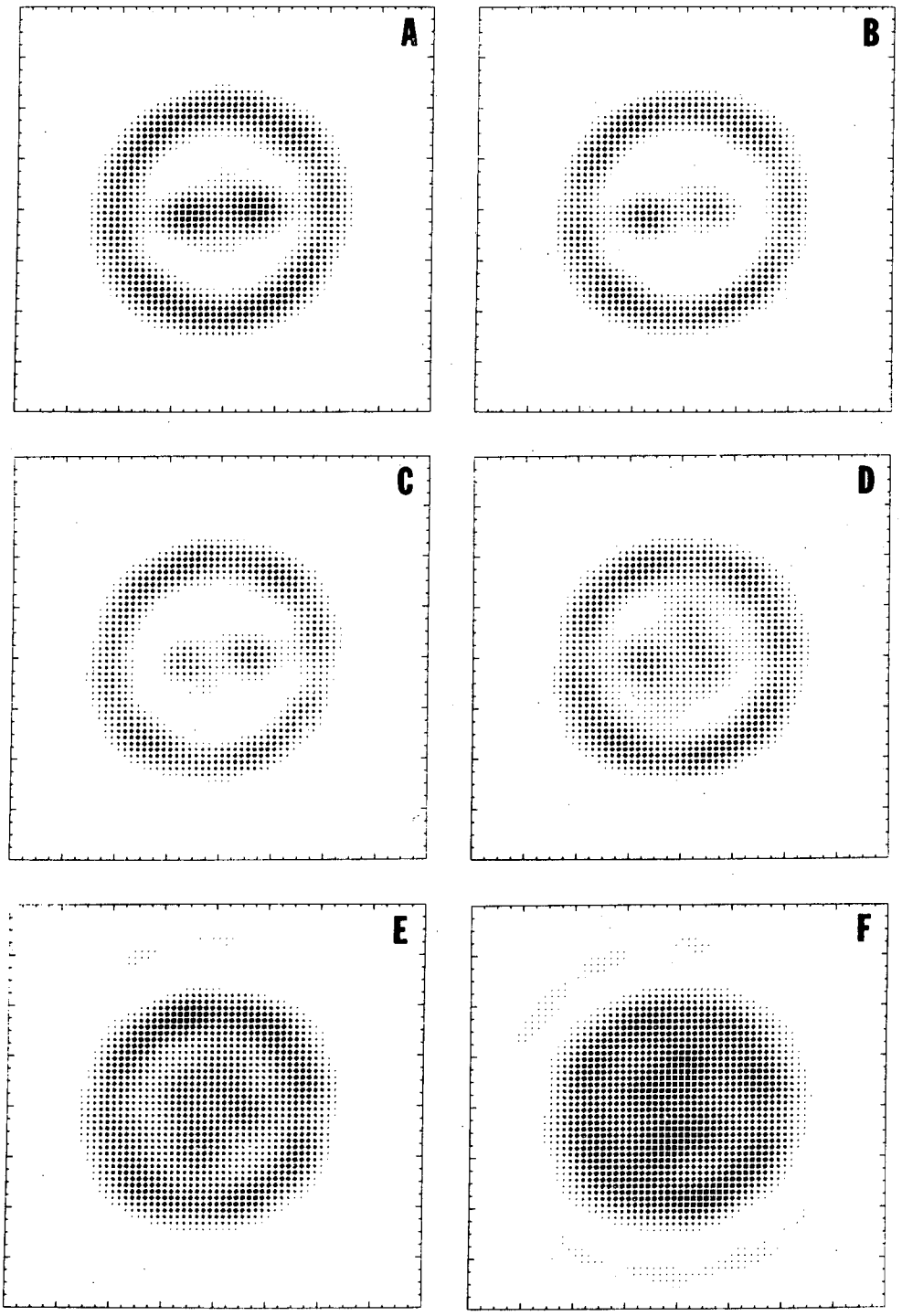

XBL 7710-10316

Fig. 12

TECHNICAL INFORMATION DEPARTMENT
LAWRENCE BERKELEY LABORATORY
UNIVERSITY OF CALIFORNIA
BERKELEY, CALIFORNIA 94720